Research Paper

68Ga-HBED-CC-PSMA PET/CT Versus Histopathology in Primary Localized Prostate Cancer: A Voxel-Wise Comparison

Constantinos Zamboglou[1]✉*, Florian Schiller[2]*, Tobias Fechter[1]*, Gesche Wieser[2], Cordula Annette Jilg[3], Alin Chirindel[4], Nasr Salman[1], Vanessa Drendel[5], Martin Werner[5], Michael Mix[2], Philipp Tobias Meyer[2]#, Anca Ligia Grosu[1]#

1. Department of Radiation Oncology, University Medical Center Freiburg, Germany; German Cancer Consortium (DKTK), Partner Site Freiburg, Germany;
2. Department of Nuclear Medicine, University Medical Center Freiburg, Germany; German Cancer Consortium (DKTK), Partner Site Freiburg, Germany;
3. Department of Urology, University Medical Center Freiburg, Germany; German Cancer Consortium (DKTK), Partner Site Freiburg, Germany;
4. Department of Nuclear Medicine, Claraspital Basel, Switzerland;
5. Department of Pathology, University Medical Center Freiburg, Germany; German Cancer Consortium (DKTK), Partner Site Freiburg, Germany.

* Contributed equally to this work

\# Contributed equally to this work

✉ Corresponding author: Constantinos Zamboglou, Department of Radiation Oncology, University Medical Center Freiburg, Germany. Robert-Koch Straße 3, D-79106 Freiburg. Telephone: +4976127094620 Telefax: +497612709582039670 Email: constantinos.zamboglou@uniklinik-freiburg.de.

Abstract

Purpose: We performed a voxel-wise comparison of 68Ga-HBED-CC-PSMA PET/CT with prostate histopathology to evaluate the performance of 68Ga-HBED-CC-PSMA for the detection and delineation of primary prostate cancer (PCa).

Methodology: Nine patients with histopathological proven primary PCa underwent 68Ga-HBED-CC-PSMA PET/CT followed by radical prostatectomy. Resected prostates were scanned by ex-vivo CT in a special localizer and histopathologically prepared. Histopathological information was matched to ex-vivo CT. PCa volume (PCa-histo) and non-PCa tissue in the prostate (NPCa-histo) were processed to obtain a PCa-model, which was adjusted to PET-resolution (histo-PET). Each histo-PET was coregistered to in-vivo PSMA-PET/CT data.

Results: Analysis of spatial overlap between histo-PET and PSMA PET revealed highly significant correlations ($p < 10^{-5}$) in nine patients and moderate to high coefficients of determination (R^2) from 42 to 82 % with an average of 60 ± 14 % in eight patients (in one patient R^2 = 7 %). Mean SUV_{mean} in PCa-histo and NPCa-histo was 5.6 ± 6.1 and 3.3 ± 2.5 ($p = 0.012$). Voxel-wise receiver-operating characteristic (ROC) analyses comparing the prediction by PSMA-PET with the non-smoothed tumor distribution from histopathology yielded an average area under the curve of 0.83 ± 0.12. Absolute and relative SUV (normalized to SUV_{max}) thresholds for achieving at least 90 % sensitivity were 3.19 ± 3.35 and 0.28 ± 0.09, respectively.

Conclusions: Voxel-wise analyses revealed good correlations of 68Ga-HBED-CC-PSMA PET/CT and histopathology in eight out of nine patients. Thus, PSMA-PET allows a reliable detection and delineation of PCa as basis for PET-guided focal therapies.

Key words: Prostate cancer, PSMA PET/CT, voxel-wise, histopathology, SUV.

Introduction

A reliable detection and delineation of the malignant tissue in the prostatic gland is necessary for risk stratification and for further treatment planning in patients with primary prostate cancer (PCa) [1]. The local spread of PCa (T-status) has an impact on D'Amico's risk criteria [2] and thus influences the

therapeutic decision process. Especially the field of focal therapy (e.g. radiotherapy, cryotherapy, laser therapy) has become of interest in the treatment of localized PCa [3]. Although PCa is a multifocal disease there is growing evidence that dominant intraprostatic lesions (DIL) within the gland may be responsible for the metastatic and recurrent disease [4, 5]. Patients suffering from low risk PCa who may be treated with active surveillance, may be also treated with focal therapy to treat the DIL only while sparing the rest of the prostate gland [6, 7]. Whereas, higher risk patients may be treated by whole-gland treatment with an additional focal dose escalation to DILs, in order to improve local tumor control [8, 9]. For focal radiation therapy target delineation, sensitivity is more important than specificity, since the entire DIL should be included in the target region. A potential over-dosage of healthy prostatic tissue should not necessarily lead to increased toxicity. A recent study could prove that even a hemigland irradiation has good dosimetric results [10].

Prior histopathologic comparative studies have shown that magnetic resonance imaging (MRI), especially when anatomical and functional MRI-information is combined, can detect primary PCa with good accuracy. For 1.5 or 3 Tesla multiparametric MRI (mpMRI), sensitivities and specificities of up to 57 – 88 % and 88 – 100% for detection of PCa have been reported [11-13]. However, MRI suffers from significant false-positive rates in benign prostatic hyperplasia [14] and more importantly has poor sensitivity in small PCa lesions, low-grade PCa as well as central prostatic gland involvement. Molecular imaging (positron emission tomography, PET) in diagnosis of primary PCa increases the performance of disease detection and may also provide a suitable tool for radiotherapy planning [15]. The role of [11]C- and ^{18}F-choline PET/CT in the diagnosis of primary PCa has been discussed controversially [16-18]. A meta-analysis reported a lesion-based, sensitivity and specificity of from 54 – 93 % and 43 - 87 %, respectively [19]. A more recent work from Bundschuh et. al [20] and our own experience [21] showed a modest discrimination of malignant and benign prostate tissue in choline PET/CT.

To increase the diagnostic value of PET in primary PCa, new radiolabelled tracers targeting the prostate-specific membrane antigen (PSMA) have been developed. Specific inhibitors are used for ligand binding to an extracellular domain of PSMA [21]. In our study we used an urea based PSMA inhibitor conjugated with thechelator HBED-CC according to Eder et al. (^{68}Ga-Glu-NH-CO-NH-Lys(Ahx)-HBED-CC) as it has shown a higher specific internalization in PCa-cells compared to DOTA-conjugates [21].

Preclinical work has demonstrated a higher PSMA expression in malignant prostate tissue compared to benign prostate tissue [22, 23] and preliminary clinical studies reported good performance of PSMA PET/CT in diagnosis of recurrent PCa [24, 25] as well as in detecting primary PCa [26-29]. Moreover, in direct comparison with ^{18}F-choline PET/CT, ^{68}Ga-HBED-CC-PSMA PET/CT illustrated a higher detection rate for recurrent PCa [24, 25] underlining the promise of this innovative technique.

For implementation of PSMA PET/CT in diagnosis and treatment planning of primary PCa a profound knowledge about the tracer accumulation in different tissue types in the prostate is necessary. This can be only achieved by an exact PET/histopathology coregistration, which would enable a voxel-wise evaluation of diagnostic performance. To our knowledge, a voxel-wise analysis has not been performed in previous studies.

Aim of this study is to evaluate spatial correlations between histopathology and ^{68}Ga-HBED-CC-PSMA PET/CT and to look for significant contrast between SUV in PCa and non-malignant tissue. The tracer performance was examined systematically in nine patients with primary PCa who underwent ^{68}Ga-HBED-CC-PSMA PET/CT before prostatectomy. A sophisticated coregistration technique allowing voxel-wise analysis between PET scans and histopathology was implemented. Due to limited spatial resolution of PSMA PET, smoothing of histopathological information was performed (histo-PET) for analyzing the spatial correspondence (R^2). Furthermore, standardized uptake values (SUV) within PCa and non-tumorous tissue including receiver-operating characteristic (ROC) curves were assessed in regions derived from the non-smoothed histopathology (clinical situation).

Patients and Methods

Patients and study design

This single institution study enrolled nine patients between February 2014 and November 2014 (Table 1). Inclusion criteria were histopathological proven primary adenocarcinoma of the prostate, pre-therapeutic ^{68}Ga-HBED-CC-PSMA PET/CT and intended radical prostatectomy. Exclusion criteria were neoadjuvant androgen deprivation therapy and previously performed transurethral resection of the prostate. Mean patient age was 63.3 years (median 64.5, range 49 - 74) and mean serum PSA at imaging was 22.4 ng/ml (median 10.8, range 5.57 - 51.13).

Three patients had intermediate and six patients had high risk PCa, according to D'Amico's risk criteria [2]. The average volume of PCa in histology was 6.76 ± 7.13 ml which was in mean 24.44 ± 23.6 % of prostatic tissue (Table 1). The volume of the largest nodule only was in average 6.21 ± 7.13 ml. Mean interval between ⁶⁸Ga-HBED-CC-PSMA PET/CT and radical prostatectomy was 19 days ± 11 (range: 1 - 42).

This study was approved by the local ethics committee and written informed consent was obtained from each patient.

Table 1. Patient characteristics

	Age (years)	PSA at imaging (ng/ml)	TNM	Epstein grading [30]	Gleason score	PCa (% of prostatic tissue)
1	67	6.07	pT3a pN1 cM0	2	7a (3+4)	28
2	52	51.13	pT3b pN1 cM0	5	9 (4+5)	42
3	59	9.15	pT2c pN0 cM0	3	7b (4+3)	4
4	60	49	pT2c pN1 cM0	2	7a (3+4)	56
5	68	11.03	pT3a pN0 cM0	2	7a (3+4)	6
6	49	5.57	pT2c pN0 cM0	1	6 (3+3)	4
7	62	47.17	pT3b pN1 cM0	4	8 (4+4)	62
8	74	8.82	pT2c pN0 cM0	2	7a (3+4)	3
9	61	10.57	pT2c pN0 cM0	2	7a (3+4)	15
Mean	61	22.06				24.44
SD ±	8	20.39				23.6

Gleason score and Eppstein grading were based on whole mount prostatectomy, respectively.

PET/CT Imaging

Glu-NH-CO-NH-Lys(Ahx)-HBED-CC was labeled with ⁶⁸GaCl₃ by using a fully automated synthesis module according to Good Laboratory Practice (Eckert & Ziegler, Germany) in combination with sterile single-use cassettes. The radiochemical purity of the final product was ≥97 % and the decay-corrected yield was >95 %.

The patients fasted for at least 4 hours before the intravenous injection of the radiopharmaceutical and were asked to void before starting the PET scan. Mean injected activity of ⁶⁸Ga-PSMA was 177 ± 37 MBq. At 1 hour post injection, patients underwent a whole body PET scan. Scans were either performed with a 64-slice GEMINI TF PET/CT or a 16-slice GEMINI TF BIG BORE PET/CT (both Philips Healthcare, USA), which provide virtually identical image characteristics [31]. To further optimize comparability of the quantitative measurements both scanners were cross-calibrated. The spatial resolution of the reconstructed PET scan is about 7 mm (full width half maximum, FWHM) for both scanners. A contrast-enhanced diagnostic CT (120 kVp, 100 - 400 mAs, dose modulation) or a low-dose CT (120 kVp, 25 mAs) for attenuation correction (depending on previous CT scans and contraindications) was performed. The accumulation of ⁶⁸Ga-PSMA-HBED-CC was quantified by standardized uptake values (SUV, regional tracer concentration normalized by injected dose and body weight).

Coregistration

A multi-step coregistration protocol between ⁶⁸Ga-HBED-CC-PSMA PET/CT and histopathology was implemented (Figure 1). In the first step, whole-mount prostate slices were coregistered to the ex-vivo CT in a manner similar to the procedure described by Grosu et al. [21]. We used a fixation device (localizer) consisting of a customized cuvette with 4-mm-spaced markers, filled with agarose in which the prostate was embedded and fixated. The basic edges (ventral, dorsal, left, right) of the resected prostate were marked with special ink to support orientation of the prostate in the agarose-filled cuvette. The aim was to position the prostate in a similar orientation as in in-vivo CT. After ex-vivo CT scan of the localizer, the pathologic slices were cut perpendicular to the urethra and along the localizer markers using a customized cutting device (Supplementary Figure 1). Parallel 4-mm step-sections were cut in the same angle as the ex-vivo CT slices. PCa and non-malignant tissue was delineated on each histopathological slice by an experienced pathologist. Histopathological slices were than manually matched to the ex-vivo CT, using MITK software (MITK Workbench 2014.10.00, German cancer research center, Germany) under guidance of the 4-mm grid. The contours of PCa (PCa-histo) and non PCa (NPCa-histo) were manually transferred to corresponding CT slices. In the next step, a careful manual coregistration with additional non-rigid deformation (to account for ex-vivo changes) between ex-vivo CT (including PCa-histo and NPCa-histo) and in-vivo CT was performed in MITK by two experienced specialists in consensus.

Subsequently, PCa-histo contours were used to represent the PCa distribution in a 4-mm slice. The voxels in a 3D model were set to discrete values (PCa 1, non PCa 0.1, tissue outside the prostatic gland 0) in PMOD (PMOD v3.6, PMOD Technologies, Switzerland). To account for the obvious (three orders of magnitude) difference between the resolution of PSMA-PET and histology slices for correlation analyses, a Gaussian smoothing (FWHM 7 mm) of the discretized histological data was performed to create a so called histo-PET. Subsequently, rigid mutual

information (MI) coregistration between PSMA PET and histo-PET was conducted in PMOD in order to account for minor in-vivo misalignments between PET and CT (i.e. due to bladder or bowel movements) and to overcome possible uncertainties between ex- and in-vivo CT coregistration (low soft-tissue contrast in CT).

VOI-based SUV analysis

Volumes of interest (VOIs) based on the coregistered histopathological information were used to analyze the PSMA-PET images. Non-smoothened PCa-histo and NPCa-histo contours were used to define separate VOIs in which SUV values were read out. In order not to bias the results because of spill-in from physiological uptake, we kept a 1-cm distance to the bladder.

Voxel-wise image analysis

By generating smoothed histo-PETs, the correlation between PET and histopathology was evaluated at a comparable image resolution, minimizing the effect of different image resolutions on spatial correspondence. The values from the histo-PETs (range 0 – 1, unit "relative SUVs") indicate the relative contribution of PCa and non-PCa to a PET voxel. For quantitative evaluation the prostate boundaries were expanded with 3 mm to take into account the spillover effect (image blurring) of PET and histo-PET. Regions of the rectum and regions around the bladder (1-cm distance) were carefully excluded to avoid a bias. The voxel-wise correlation between PSMA-PET (in SUV) versus histo-PET (in relative SUV) was evaluated qualitatively by visual inspection of scatterplots and quantitatively by linear regression providing the coefficient of determination (R^2) and its statistical significance (p values). On average, 4496 ± 1241 voxels (range 3128 to 6447) with a voxel-size of 2x2x2 mm^3 were analyzed per patient. .

Receiver-operating characteristic (ROC) analyses evaluating sensitivity and specificity of PSMA PET as a function of a SUV threshold were performed for all patients within the same expanded VOIs as the scatterplots in Figure 3. In contrast to the latter, non-smoothed, binarized histopathology models have to be used in order to reflect the clinical situation.

Statistical Analyses

SPSS (Version 23, IBM, USA) was used for Wilcoxon Test and to calculate Spearmans Rho. Linear regression (t-statistics) and ROC analyses were performed in MATLAB (MATLAB R2014a, The MathWorks, USA). P-values < 0.05 were considered statistically significant.
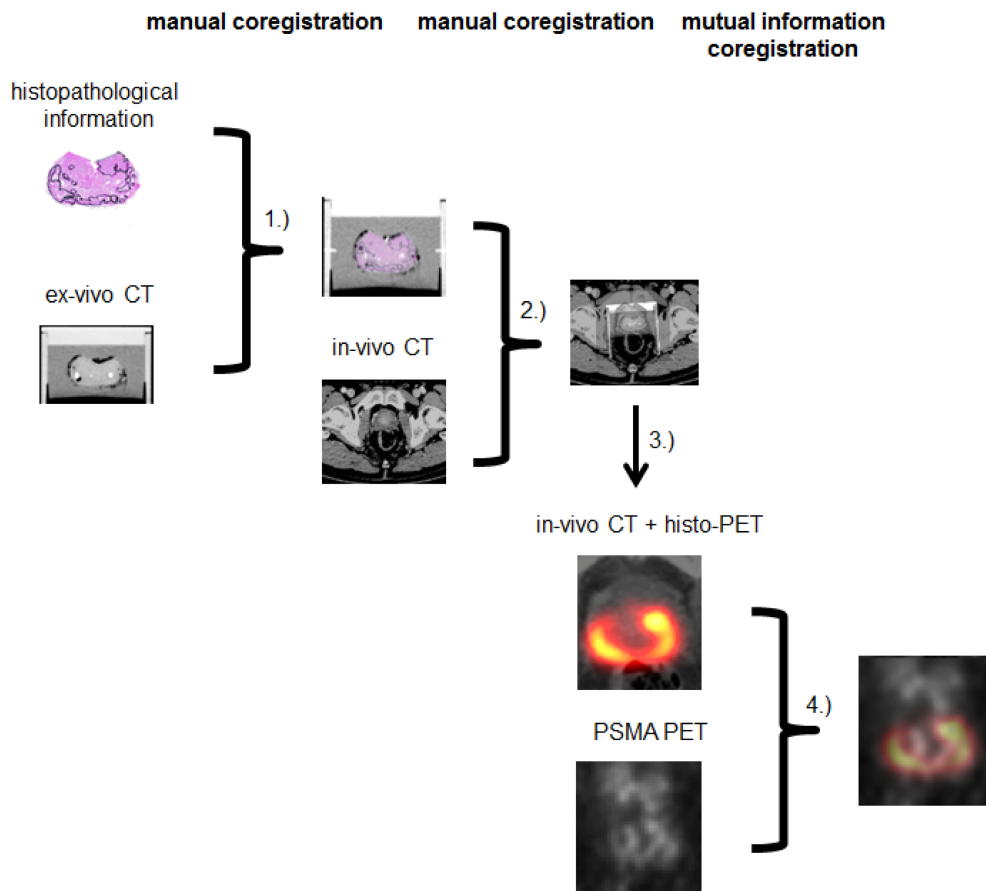

Figure 1. Coregistration between step sections and ex-vivo CT was done by CZ in MITK (1). Ex-vivo CT (including histopathology) was matched to in-vivo CT by CZ and AC in MITK (2). Histopathological information was interpolated, binarized and smoothed to create histo-PET (3). Using rigid mutual information histo-PET and PSMA PET were coregistrated in PMOD (4).

Results

Tracer uptake in PCa and non PCa tissue

The average SUVmean in PCa-histo and NPCa-histo VOIs after coregistration was 5.6 ± 6.1 (range: 1.6 - 21) and 3.3 ± 2.5 (range: 1.5 – 8.4) (paired Wilcoxon test, p = 0.012, Figure 2), respectively. The SUVmean ratio in the VOIs of PCa-histo and NPCa-histo was 1.6 ± 0.6 (range: 0.9 - 2.5).

In six of nine patients (66.7 %), the SUVmax of PSMA PET was located within the coregistered PCa-histo. Correlations between postoperative Gleason score, intraprostatic tumor burden and PSA serum value with SUVmean in PCa-histo did not reach a level of significance (p = 0.1, p = 0.1 and p = 0.08, respectively), see Figure 3.

Spatial overlap between ^{68}Ga-HBED-CC-PSMA PET/CT and histopathology

Visual evaluation showed moderate to good overlap between PET and histopathology in eight of nine patients, with the exception of patient five (Figure 4). Voxel-wise analysis of spatial agreement between PSMA PET and histo-PET revealed mean R^2 of 55 % ± 16 % (median 57 %, range: 7 - 82 %, p < 10^{-5} for all, Figure 5).

ROC analyses revealed areas under curves (AUCs) of up to 0.94 with an average of 0.83 ± 0.12 (Figure 6). The best SUV threshold of the PSMA PET was determined by requesting a sensitivity of ≥0.90 (Table 2). The absolute SUV threshold was in average 3.19 ± 3.35. Furthermore, relative thresholds normalized to the SUVmax (over five pixels) in the examined volume were calculated. The best relative threshold was in mean 0.28 ± 0.09. The combination of all voxels of all patients into one dataset yielded a best SUV threshold at 1.89.
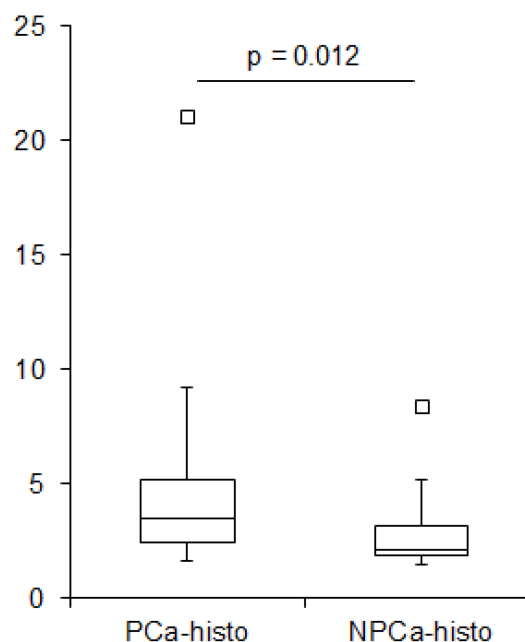

Figure 2. Boxplot showing SUVmean values in PCa-histo and NPCa-histo. The first (Q1) and the third (Q3) quartile are the bottom and the top of the box. The medians (horizontal line inside box) for PCa-histo and NPCa-histo were 3.5 and 2.1, respectively. The ends of the whisker are set at 1.5xIQR (interquartile range) above Q3 and 1.5xIQR below Q1. Black quadrat: upper outliner.

Table 2. Overview of ROC analyses

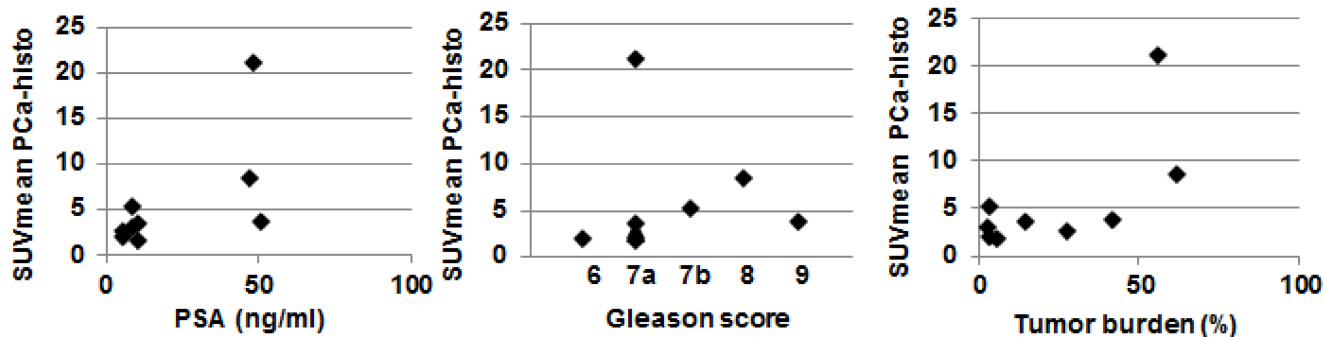| Patient	AUC	Best absolute threshold [SUV] for Sensitivity ≥ 0.90	Relative threshold of SUVmax	Corresp. Specificity
1	0.76	1.58	0.24	0.48
2	0.84	1.68	0.21	0.55
3	0.92	2.05	0.18	0.69
4	0.91	11.49	0.21	0.72
5	0.56	1.19	0.21	0.31
6	0.76	1.39	0.37	0.60
7	0.90	5.35	0.34	0.79
8	0.94	1.93	0.46	0.81
9	0.88	2.01	0.29	0.67
Mean	0.83 ± 0.12	3.19 ± 3.35	0.28 ± 0.09	

Figure 3. Scatterplot showing the correlation between SUVmean in PCa-histo with clinical parameters. Spearmans Rho test showed no statistically significant correlation for PSA serum value (rho = 0.6, p = 0.08), postoperative Gleason score (rho = 0.58, p = 0.1) and Tumor burden (rho = 0.58, p = 0.1).
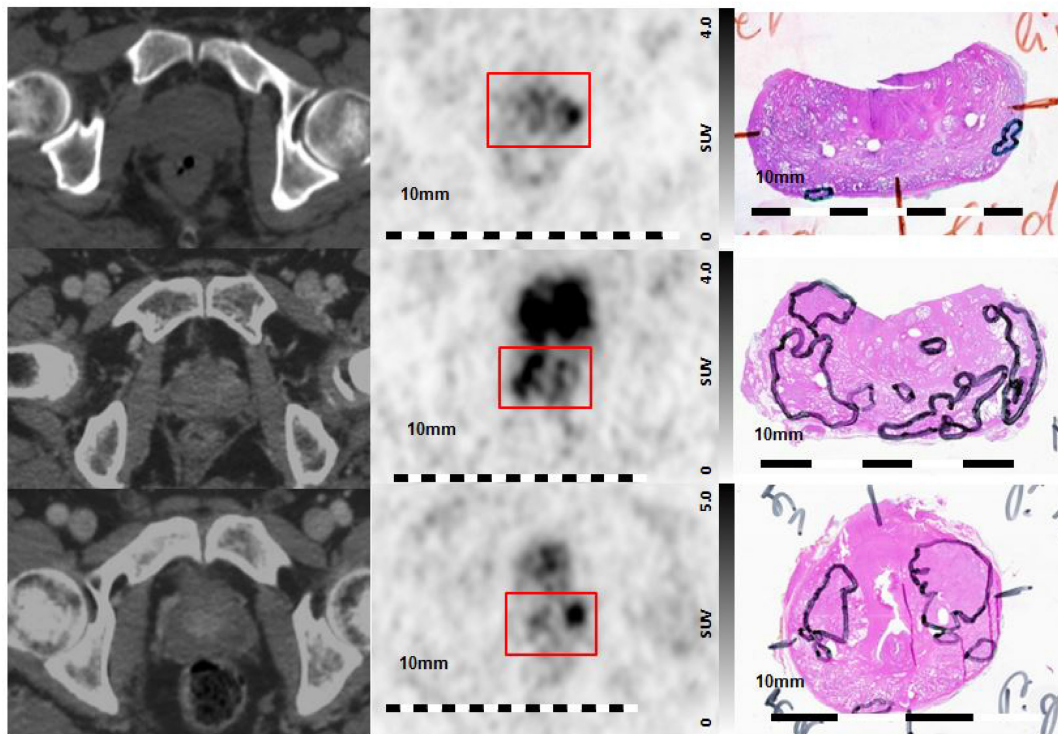
Figure 4. Visual Evaluation of spatial correlation between PSMA PET and histopathology. Step sections were coregistered to 68Ga-HBED-CC-PSMA PET images Left column: axial CT images, middle column: corresponding axial 68Ga-HBED-CC-PSMA PET images, right column: corresponding histopathological slices (manual coregistration). Upper line: poor overlap between PET and histopathology in patient 5. Note the small and lentiform shaped tumors. Middle line: good overlap of PET and histopathology in patients 1, and lower line: moderate overlap in patient 9. Red box: area of prostatic gland in PET images.
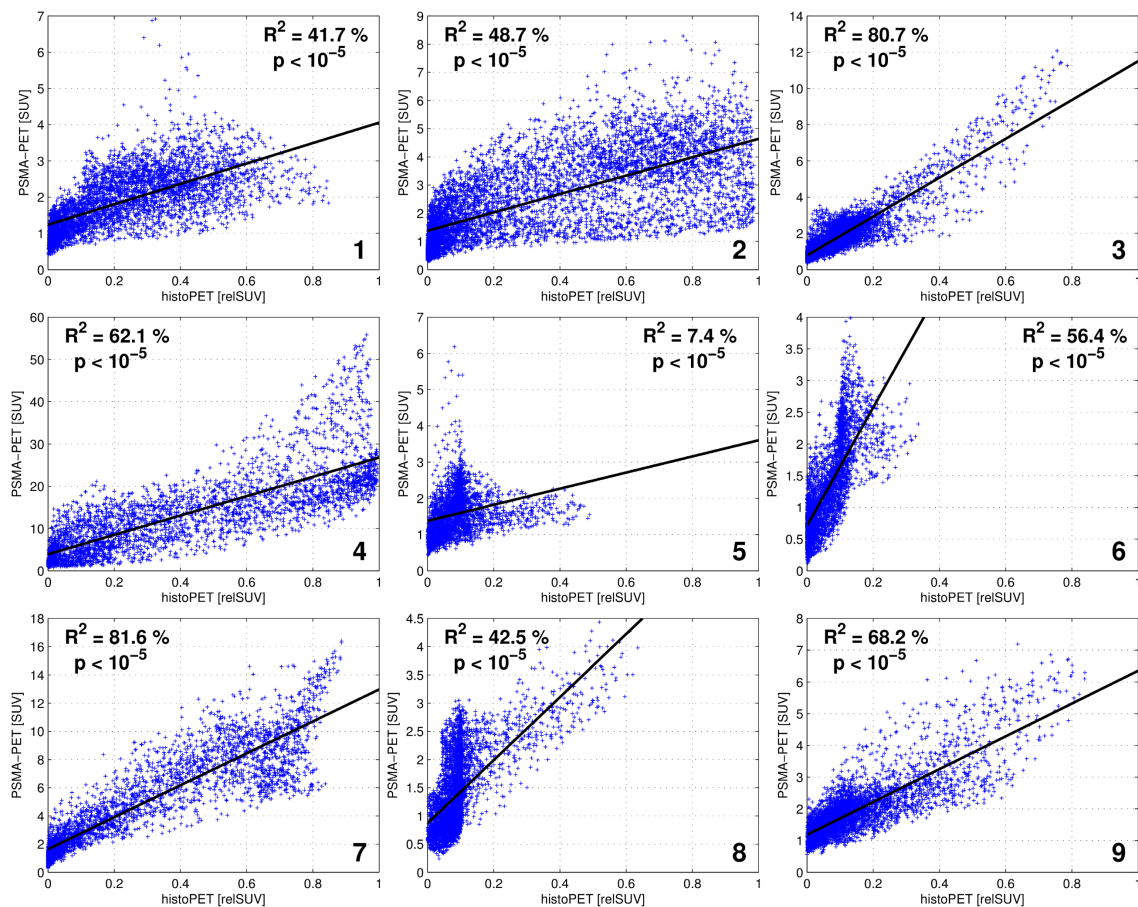

Figure 5. Scatterplots showing the correlation between SUV of 68Ga-HBED-CC-PSMA PET and relSUV of histo-PET for Patient 1 – 9.
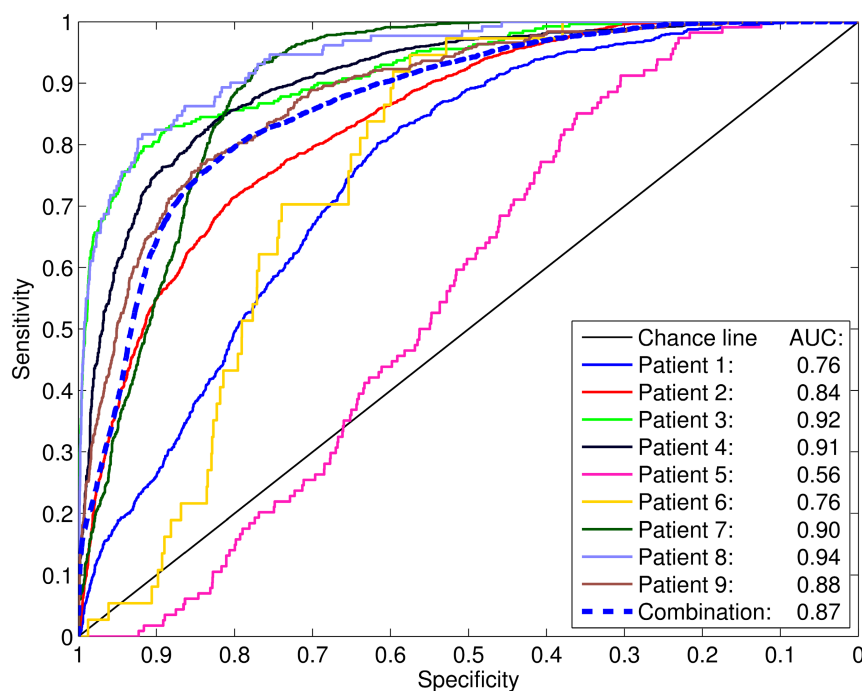
Figure 6. For each patient, the PSMA-PET was compared to the coregistered, binarized (i.e. not smoothed) histopathology model in a ROC analysis. The areas under curve (AUC) are indicated. The dashed "combination" line represents the ROC analysis including all voxels of all patients combined into a single dataset.

Discussion

To the best of our knowledge, this is the first study to evaluate the value of ^{68}Ga-HBED-CC-^{68}Ga-HBED-CC-PSMA PET/CT in comparison to histopathology for primary PCa in a well-controlled coregistration system. The analysis was carried to a voxel level with the goal to quantitatively compare PSMA PET with histopathology and to assess its potential as a platform for defining target volumes to guide focal therapy.

Recently, three clinical studies correlated PSMA PET/CT to histopathology in patients with primary PCa. Rowe et al., performed a per-segment analysis and demonstrated 17 % sensitivity and 96 % specificity for ^{18}F-DCFBC PET/CT in detecting primary PCa. Additionally, it appears that ^{18}F-DCFBC-PSMA-PET/CT can detect clinically significant high-grade PCa with higher specificity than MRI [27]. One current study including 6 patients reported 92 % sensitivity and specificity for ^{68}Ga-PSMA-HBED-CC based on visual coregistration and analysis in 24 prostate segments (including seminal vessels). Furthermore, they showed that SUVmax was significantly higher in segments with true positive PSMA signal then in segments with true negative PSMA signal [29]. Eiber et al., compared ^{68}Ga-HBED-CC-PSMA PET/MRI with histopathology in 53 patients on a sextant basis. They reported AUC values for mpMRI, PSMA PET and PSMA-PET/MRI of 0.73, 0.83 and 0.88, respectively [32].

Non-linear deformations occur in the prostate in-vivo due to rectum and bladder filling. The loss of blood volume and the histopathological work-up ex-vivo lead to inhomogeneous shrinkage throughout different regions of the prostate [33]. Bundschuh et al., calculated a mean shrinkage factor of 0.79 ± 0.16 between prostate volume in in-vivo and ex-vivo CT scans [20]. These deformations impede direct manual coregistration of histology sections and *PET/CT*. Further uncertainty in coregistration is caused by differences in resolution between PET, CT and MRI imaging (e.g., resolution in millimeters) and histology (e.g., resolution in microns) [33]. Additionally, the axial planes of the patients CT scan may not have the same cutting angle as the histopathology slices. Up to date there is limited experience in PSMA-based PCa-definition, since the determination of malignant PSMA uptake is based on a subjective interpretation by the reader [34]. Considering these uncertainties, solely visual coregistration and correlation between PSMA PET/CT images and histopathology may not be sufficient for evaluation.

Thus, we implemented a non-rigid CT based coregistration between in-vivo and ex-vivo scans combined with rigid MI between histo-PET and PSMA PET. The implementation of a localizer and the usage of a cutting device resulted in pathological slices directly corresponding to ex-vivo CT slices. However, a potential distortion of the gland between in-vivo imaging and ex-vivo slicing remained. Implementation of a custom made prostate mold as

performed by Trivedi et al. [35] may serve as a possible solution. Another approach for better alignment between in-vivo and ex-vivo data was presented by Orczyk et al. [36], who created a 3D model of histology which was matched to MRI data by MI coregistration. By processing histopathological data into 3D histo-PET models, we were able to take into account physical properties of PET (i.e. partial volume effects) and to create a 3D counterpart within the same reference space. The non-rigid manual coregistration step is a prerequisite, since it aligns in-vivo with ex-vivo CT in anatomical plausible boundaries, taking into account the non-linear deformations due to histopathological work-up. Subsequent MI between the 3D patterns of PET and histo-PET was performed to overcome possible uncertainties of solely CT-based registration. The voxel-wise evaluation of pattern agreement revealed that eight patients had moderate to high R^2-values (42 - 82 %), whereas one patient (number 5) had low R^2 of 7 %, with $p < 10^{-5}$ for all patients.

Patient 5 had similar clinical characteristics as the other patients (Table 1) but were characterized by several small and lentiform PCa lesions in histopathology. Visual correlation between PSMA PET and histopathology (Figure 4, upper row) revealed a small left peripheral lesion on histology, while the left-sided PET focus appeared disporportionally large. The lesion on the right side was missed by PET. This disagreement can also be appreciated by inspection of the scatter plot in Figure 5, showing corresponding vertical and horizontal extensions, respectively. The lack of detection of the very small, lentiform right-sided lesion may be explained by PET resolution limitation [37], while the discrepantly larger PET focus on the left side could be due to incomplete histopathological coverage. Small-size lesions with less than 4-mm thickness (distance between two step-sections) may not be appropriately covered by histopathology, while still causing focal uptake on PET.

SUVmean values were significantly higher in PCa-histo compared to NPCa-histo. This is consistent with two current studies [29, 32] which reported a high uptake ratio between malignant versus nonmalignant tissues on a segment basis. Furthermore, we obtained similar AUC values, sensitivities, and specificities as the latter studies, although a much more coarse comparison was performed in these studies. We showed a good prediction of malignant tissue by PSMA PET found for most patients in the ROC analyses with AUCs up to 0.94. This is remarkable since the intrinsic resolution of PET was not taken into account for these analyses in order to reflect the clinical situation. The

intrinsic PET resolution may thus result in an SUVmax of a certain lesion lying outside the intial PCa volume [37]. In particular, this is an issue for small lesions. In 6 patients SUVmax of 68Ga-HBED-CC-PSMA PET was located in PCa-histo. The 3 patients with SUVmax outside PCa-histo showed middle to small sized lesions (maximal axial diameter 1mm – 16 mm). This result may be a direct consequence of the PCa geometry in combination with partial-volume effect and statistical noise [38] and not necessarily due to a poor tracer performance.

Particularly in patients with moderate to high R^2-values, high tumor to background ratios as well as ROCs with very good AUC were measured. This is a prerequisite for possible PET-guided focal therapy approaches in PCa. To enable an objective definition of the target volume, algorithms based on a SUV-threshold for PSMA PET may be used [39].

The scatter among the patients regarding best SUV thresholds according to the 0.9-sensitivity criterium (3.19 ± 3.35) was of the order of the mean threshold (relative standard deviation 1.05). This heterogeneous picture may be due to the difference in the tumor biology, non-specific influences on tracer binding like its perfusion as well as geometry, or the used methodology. Interestingly, the situation seems considerably more homogeneuos when assessing relative thresholds normalized to the SUVmax (over 5 pixels) in the examined volume. With that, the best relative thresholds were 0.28 ± 0.09, which reduces the relative standard deviations to 0.33. This is close to a relative threshold of 0.41 suggested for volume quantification in FDG-PET [40].

An ROC analysis of the voxels of all patients combined into one dataset yields a best SUV threshold at 1.89. Applying this commonthreshold to each patient individually reveals highly variable sensitivities from 0.25 to 1.00 and specificities from 0.08 to 0.77. This would indicate that radiation planning based on (PSMA-)PET using a general threshold is likely to either miss a pronounced fraction of PCa tissue or burden considerably more tissue than necessary. Although a larger cohort is necessary for verification, our findings point towards a relative SUV threshold around 30 % of SUVmax in the prostate, which may be used for PSMA based target delineation to guide focal therapy approaches. Furthermore, the promising results in our study may suggest a usage of 68Ga-HBED-CC-PSMA PET/CT in initial diagnosis and active surveillance of primary PCa.

Unlike previous studies [27, 29, 41], we did not detect a clear significant correlation between SUVmean in coregistered PCa volumes and PSA serum value, Gleason score or tumor burden,

respectively. This may be due to the limited number of cases and relatively small variability, since 5 of nine patients had a Gleason 7a (3+4). In high-risk patients with multifocal disease, the delineation of the lesion with the highest SUVmean may help to guide a dose escalation on the potential DIL in addition to whole gland treatment. However, a good spatial correlation between PSMA PET and histopathology was also observed in one patient with Gleason score 6 and in five patients with Gleason score 7a (R^2 = 50.4 ± 25.9), in which Gleason 3 patterns are predominant. This finding is consistent with two studies [29, 32], which could show that PSMA PET has a good spatial correlation with histopathology in patients with low-grade PCa. In low-risk PCa patients, the knowledge of Gleason 3 extent would help to guide focal therapy on DIL only and may serve as a tool for active surveillance as well. Recently, Rowe et al. defined the DIL as the lesion with the highest Gleason score. A DIL-based analysis resulted in an increased performance of ^{18}F-DCFBC PET/CT (sensitivity increased from 17 to 46 %, while specificity remained largely unchanged) compared to the global segment based approach [27]. Since there is no definitive data on which parameters the DIL should be defined [42, 43], no separate analysis of a DIL was performed in our study. Our coregistration protocol enables potential further correlation between various histopathological procedures (e.g. immunohisto-chemistry, immunofluorescence, autoradiography) and PET/CT images. From these, future work could examine if ^{68}Ga-HBED-CC-PSMA PET accurately detects the DIL.

This study has several limitations. First limitation is the relatively low number of patients, which was preferable to our elaborate coregistration and evaluation protocol. Despite the implementation of a sophisticated coregistration pathway several uncertainties in correlation of PET and histopathology remain. Thus, it could not be excluded that moderate R^2 or AUC (ROC curve) values or low tumor to background ratios are consequences of mismatch in coregistration or incomplete histopathological coverage instead of poor tracer performance. The PET-based MI relies on the patterns of histo-PET and PSMA PET. Thus, the result of MI coregistration was controlled to ensure that only anatomical plausible transformations occured. Shifts of up to two times FWHM of the PET resolution (i.e. 14 mm) were considered as plausible.

Conclusion

Voxel-wise analysis revealed a good correlation (R^2, ROC AUC) between ^{68}Ga-PSMA-PET/CT and the histopathological goldstandard in eight of nine patients. This underlines the suitability of PSMA as tracer for primary prostate cancer. Our findings do not support a general SUV threshold for delineating PCa in PSMA-PET for focal therapy but seem to point towards a relative threshold around 30 % of SUVmax.

Supplementary Material

Supplementary Figure S1.
http://www.thno.org/v06p1619s1.pdf

Abbreviations

PCa: prostate cancer; MRI: magnetic resonance imaging; mpMRI: multiparametric MRI; PET: positron emission tomography; PSMA: prostate-specific membrane antigen; SUV: standardized uptake values; ROC: receiver-operating characteristic; VOI: volume of interest; DIL: dominant intraprostatic lesion; MI: mutual information.

Competing Interests

References

1. Heidenreich A, Bastian PJ, Bellmunt J, Bolla M, Joniau S, van der Kwast T, et al. EAU guidelines on prostate cancer. part 1: screening, diagnosis, and local treatment with curative intent-update 2013. Eur Urol. 2014; 65: 124-37.
2. D'Amico AV, Desjardin A, Chung A, Chen MH. Assessment of outcome prediction models for localized prostate cancer in patients managed with external beam radiation therapy. Semin Urol Oncol. 1998; 16: 153-9.
3. Valerio M, Ahmed HU, Emberton M, Lawrentschuk N, Lazzeri M, Montironi R, et al. The role of focal therapy in the management of localised prostate cancer: a systematic review. Eur Urol. 2014; 66: 732-51.
4. Pucar D, Hricak H, Shukla-Dave A, Kuroiwa K, Drobnjak M, Eastham J, et al. Clinically significant prostate cancer local recurrence after radiation therapy occurs at the site of primary tumor: magnetic resonance imaging and step-section pathology evidence. Int J Radiat Oncol Biol Phys. 2007; 69: 62-9.
5. Bott SR, Ahmed HU, Hindley RG, Abdul-Rahman A, Freeman A, Emberton M. The index lesion and focal therapy: an analysis of the pathological characteristics of prostate cancer. BJU Int. 2010; 106: 1607-11.
6. Bauman G, Haider M, Van der Heide UA, Menard C. Boosting imaging defined dominant prostatic tumors: a systematic review. Radiother Oncol. 2013; 107: 274-81.
7. Mouraviev V, Villers A, Bostwick DG, Wheeler TM, Montironi R, Polascik TJ. Understanding the pathological features of focality, grade and tumour volume of early-stage prostate cancer as a foundation for parenchyma-sparing prostate cancer therapies: active surveillance and focal targeted therapy. BJU Int. 2011; 108: 1074-85.
8. Lips IM, van der Heide UA, Haustermans K, van Lin EN, Pos F, Franken SP, et al. Single blind randomized phase III trial to investigate the benefit of a focal lesion ablative microboost in prostate cancer (FLAME-trial): study protocol for a randomized controlled trial. Trials. 2011; 12: 255.

9. Nguyen PL, Chen MH, Zhang Y, Tempany CM, Cormack RA, Beard CJ, et al. Updated results of magnetic resonance imaging guided partial prostate brachytherapy for favorable risk prostate cancer: implications for focal therapy. J Urol. 2012; 188: 1151-6.

10. Kishan AU, Park SJ, King CR, Roberts K, Kupelian PA, Steinberg ML, et al. Dosimetric benefits of hemigland stereotactic body radiotherapy for prostate cancer: implications for focal therapy. Br J Radiol. 2015; 88: 20150658.

11. Turkbey B, Pinto PA, Mani H, Bernardo M, Pang Y, McKinney YL, et al. Prostate cancer: value of multiparametric MR imaging at 3 T for detection--histopathologic correlation. Radiology. 2010; 255: 89-99.

12. Tan CH, Hobbs BP, Wei W, Kundra V. Dynamic contrast-enhanced MRI for the detection of prostate cancer: meta-analysis. AJR Am J Roentgenol. 2015; 204: W439-48.

13. de Rooij M, Hamoen EH, Futterer JJ, Barentsz JO, Rovers MM. Accuracy of multiparametric MRI for prostate cancer detection: a meta-analysis. AJR Am J Roentgenol. 2014; 202: 343-51.

14. Bonekamp D, Jacobs MA, El-Khouli R, Stoianovici D, Macura KJ. Advancements in MR imaging of the prostate: from diagnosis to interventions. Radiographics. 2011; 31: 677-703.

15. Bentzen SM, Gregoire V. Molecular imaging-based dose painting: a novel paradigm for radiation therapy prescription. Semin Radiat Oncol. 2011; 21: 101-10.

16. Kwee SA, Wei H, Sesterhenn I, Yun D, Coel MN. Localization of primary prostate cancer with dual-phase 18F-fluorocholine PET. J Nucl Med. 2006; 47: 262-9.

17. Farsad M, Schiavina R, Castellucci P, Nanni C, Corti B, Martorana G, et al. Detection and localization of prostate cancer: correlation of (11)C-choline PET/CT with histopathologic step-section analysis. J Nucl Med. 2005; 46: 1642-9.

18. Chang JH, Joon DL, Lee ST, Gong SJ, Scott AM, Davis ID, et al. Histopathological correlation of (11)C-choline PET scans for target volume definition in radical prostate radiotherapy. Radiother Oncol. 2011; 99: 187-92.

19. Umbehr MH, Muntener M, Hany T, Sulser T, Bachmann LM. The role of 11C-choline and 18F-fluorocholine positron emission tomography (PET) and PET/CT in prostate cancer: a systematic review and meta-analysis. Eur Urol. 2013; 64: 106-17.

20. Bundschuh RA, Wendl CM, Weirich G, Eiber M, Souvatzoglou M, Treiber U, et al. Tumour volume delineation in prostate cancer assessed by [11C]choline PET/CT: validation with surgical specimens. Eur J Nucl Med Mol Imaging. 2013; 40: 824-31.

21. Grosu AL, Weirich G, Wendl C, Prokic V, Kirste S, Geinitz H, et al. 11C-Choline PET/pathology image coregistration in primary localized prostate cancer. Eur J Nucl Med Mol Imaging. 2014; 41: 2242-8.

22. Mhawech-Fauceglia P, Zhang S, Terracciano L, Sauter G, Chadhuri A, Herrmann FR, et al. Prostate-specific membrane antigen (PSMA) protein expression in normal and neoplastic tissues and its sensitivity and specificity in prostate adenocarcinoma: an immunohistochemical study using mutiple tumour tissue microarray technique. Histopathology. 2007; 50: 472-83.

23. Silver DA, Pellicer I, Fair WR, Heston WD, Cordon-Cardo C. Prostate-specific membrane antigen expression in normal and malignant human tissues. Clin Cancer Res. 1997; 3: 81-5.

24. Eiber M, Maurer T, Souvatzoglou M, Beer AJ, Ruffani A, Haller B, et al. Evaluation of Hybrid 68Ga-PSMA Ligand PET/CT in 248 Patients with Biochemical Recurrence After Radical Prostatectomy. J Nucl Med. 2015; 56: 668-74.

25. Ceci F, Uprimny C, Nilica B, Geraldo L, Kendler D, Kroiss A, et al. Ga-PSMA PET/CT for restaging recurrent prostate cancer: which factors are associated with PET/CT detection rate? Eur J Nucl Med Mol Imaging. 2015.

26. Kabasakal L, Demirci E, Ocak M, Akyel R, Nematyazar J, Aygun A, et al. Evaluation of PSMA PET/CT imaging using a 68Ga-HBED-CC ligand in patients with prostate cancer and the value of early pelvic imaging. Nucl Med Commun. 2015; 36: 582-7.

27. Rowe SP, Gage KL, Faraj SF, Macura KJ, Cornish TC, Gonzalez-Roibon N, et al. 18F-DCFBC PET/CT for PSMA-Based Detection and Characterization of Primary Prostate Cancer. J Nucl Med. 2015; 56: 1003-10.

28. Budaus L, Leyh-Bannurah SR, Salomon G, Michl U, Heinzer H, Huland H, et al. Initial Experience of Ga-PSMA PET/CT Imaging in High-risk Prostate Cancer Patients Prior to Radical Prostatectomy. Eur Urol. 2015.

29. Rahbar K, Weckesser M, Huss S, Semjonow A, Breyholz HJ, Schrader AJ, et al. Correlation of intraprostatic tumor extent with 68-Ga-PSMA distribution in patients with prostate cancer. J Nucl Med. 2016.

30. Epstein JI, Zelefsky MJ, Sjoberg DD, Nelson JB, Egevad L, Magi-Galluzzi C, et al. A Contemporary Prostate Cancer Grading System: A Validated Alternative to the Gleason Score. Eur Urol. 2016; 69: 428-35.

31. Scheuermann JS, Surti S, Kolthammer JA, Karp JS. Evaluation of a fully 3D, big bore TOF PET scanner with reduced scatter shields. 2009 Ieee Nuclear Science Symposium Conference Record, Vols 1-5. 2009: 3589-92.

32. Eiber M, Weirich G, Holzapfel K, Souvatzoglou M, Haller B, Rauscher I, et al. Simultaneous Ga-PSMA HBED-CC PET/MRI Improves the Localization of Primary Prostate Cancer. Eur Urol. 2016.

33. Park H, Piert MR, Khan A, Shah R, Hussain H, Siddiqui J, et al. Registration methodology for histological sections and in vivo imaging of human prostate. Acad Radiol. 2008; 15: 1027-39.

34. Zamboglou C, Wieser G, Hennies S, Rempel I, Kirste S, Soschynski M, et al. MRI versus Ga-PSMA PET/CT for gross tumour volume delineation in radiation treatment planning of primary prostate cancer. Eur J Nucl Med Mol Imaging. 2015.

35. Trivedi H, Turkbey B, Rastinehad AR, Benjamin CJ, Bernardo M, Pohida T, et al. Use of patient-specific MRI-based prostate mold for validation of multiparametric MRI in localization of prostate cancer. Urology. 2012; 79: 233-9.

36. Orczyk C, Rusinek H, Rosenkrantz AB, Mikheev A, Deng FM, Melamed J, et al. Preliminary experience with a novel method of three-dimensional co-registration of prostate cancer digital histology and in vivo multiparametric MRI. Clin Radiol. 2013; 68: e652-8.

37. Souvatzoglou M, Weirich G, Schwarzenboeck S, Maurer T, Schuster T, Bundschuh RA, et al. The sensitivity of [11C]choline PET/CT to localize prostate cancer depends on the tumor configuration. Clin Cancer Res. 2011; 17: 3751-9.

38. Akamatsu G, Ikari Y, Nishida H, Nishio T, Ohnishi A, Maebatake A, et al. Influence of Statistical Fluctuation on Reproducibility and Accuracy of SUVmax and SUVpeak: A Phantom Study. J Nucl Med Technol. 2015; 43: 222-6.

39. Shepherd T, Teras M, Beichel RR, Boellaard R, Bruynooghe M, Dicken V, et al. Comparative study with new accuracy metrics for target volume contouring in PET image guided radiation therapy. IEEE Trans Med Imaging. 2012; 31: 2006-24.

40. Krohn T, Kaiser HJ, Gagel B, Boy C, Schaefer WM, Buell U, et al. [3D volume and SUV analysis of oncological PET studies: a voxel-based image processing tool with NSCLC as example]. Nuklearmedizin. 2007; 46: 141-8.

41. Morigi JJ, Stricker PD, van Leeuwen PJ, Tang R, Ho B, Nguyen Q, et al. Prospective Comparison of 18F-Fluoromethylcholine Versus 68Ga-PSMA PET/CT in Prostate Cancer Patients Who Have Rising PSA After Curative Treatment and Are Being Considered for Targeted Therapy. J Nucl Med. 2015; 56: 1185-90.

42. Ravery V, Chastang C, Toublanc M, Boccon-Gibod L, Delmas V, Boccon-Gibod L. Percentage of cancer on biopsy cores accurately predicts extracapsular extension and biochemical relapse after radical prostatectomy for T1-T2 prostate cancer. Eur Urol. 2000; 37: 449-55.

43. Haffner MC, Mosbruger T, Esopi DM, Fedor H, Heaphy CM, Walker DA, et al. Tracking the clonal origin of lethal prostate cancer. J Clin Invest. 2013; 123: 4918-22.